Upconversion luminescence, intrinsic optical bistability, and optical thermometry in Ho^{3+}/Yb^{3+}: $BaMoO_4$ phosphors

Xin Liu (刘 鑫), Ruoshan Lei (雷若姗)*, Feifei Huang (黄飞飞), Degang Deng (邓德刚), Huanping Wang (王焕平), Shilong Zhao (赵士龙), and Shiqing Xu (徐时清)**

College of Materials Science and Engineering, China Jiliang University, Hangzhou 310018, China
**Corresponding author: leiruo@163.com; **corresponding author: sxucjlu@163.com*
Received May 14, 2019; accepted June 26, 2019; posted online September 4, 2019

Ho^{3+}/Yb^{3+}: $BaMoO_4$ phosphors with different concentrations were fabricated by a gel combustion method. The upconversion (UC) luminescence, intrinsic optical bistability, and the corresponding mechanisms were reported for the present system. The optical thermometric properties based on red ($^5F_5 \rightarrow {}^5I_8$) and green ($^5F_4/{}^5S_2 \rightarrow {}^5I_8$) emissions were studied. The sensing sensitivities could be tuned by manipulating the cooperative energy transfer process. The highest absolute sensitivity was $99 \times 10^{-4}\ K^{-1}$ at 573 K, which is larger than that of many previous UC materials.

OCIS codes: 160.5690, 120.6780, 280.4788.
doi: 10.3788/COL201917.111601.

Rare earth (RE)-doped upconversion (UC) luminescent materials are extensively studied due to their wide applications in bio-imaging, color displays, optical thermometers, optical logic gates, and so on[1–5]. Particularly, the optical thermometry based on the fluorescence intensity ratio (FIR) of UC materials has attracted growing attentions for its advantages of high spatial resolution, noncontact operation, rapid response, etc., which is suitable for harsh measurement conditions or moving objects[2,3]. In most cases, the FIR technique determines temperature via two thermally coupled levels (TCLs) of RE ions, which suffers from the disadvantages of low signal discriminability and temperature resolution, owing to the small energy gaps between TCLs[6,7]. Actually, the FIR between two non-TCLs of RE elements can also be considered as the thermometric parameter. However, the relevant reports are still scarce, not to mention the tunability of sensing behaviors based on non-TCLs.

Besides, intrinsic optical bistability (IOB) is another attractive property observed in some UC materials, in which the emission obeys a hysteresis behavior upon increasing/decreasing pump power. By far, IOB has been investigated in several Yb^{3+}, Er^{3+}/Yb^{3+}, and Tm^{3+}/Yb^{3+}-doped materials, which are suggested to be applicable to optical gates, optical transistors, and so on[8–10]. However, the IOB process in Ho^{3+}/Yb^{3+}: $BaMoO_4$ phosphor has not been reported, to our knowledge.

In this Letter, $BaMoO_4$ is selected as the host material due to its reasonable phonon frequency (~800 cm^{-1}), good chemical and physical stability, high anti-humidity characteristics, and so on[11–13]. The UC luminescence, IOB, and temperature sensing behaviors of Ho^{3+}/Yb^{3+}: $BaMoO_4$ phosphors were studied. The tunability of sensing sensitivity based on $^5F_5$ and $^5F_4/{}^5S_2$ levels of Ho^{3+} ions was presented, and its relation with excitation power was discussed.

$BaMoO_4$ powders doped with 0.5 mol% Ho^{3+} and x mol% Yb^{3+} were prepared by a gel combustion method, where $x = 3$, 5, 7, and 10. The raw materials of $Ba(NO_3)_3$ (99.99%), Na_2MoO_4 (A.G.), $Ho(NO_3)_3 \cdot 5H_2O$ (99.99%), and $Yb(NO_3)_3 \cdot 5H_2O$ (99.99%) were dissolved in deionized water, respectively. These solutions were mixed with the appropriate amount, and then glycine was added with the nitrate to glycine ratio of 1:4. The mixed solution was heated at 90°C to form a gel, which was then heated at 400°C for 2 h. Finally, the precursor powders were calcined at 800°C for 2 h to obtain the product. The phase composition of the samples was determined by X-ray diffraction (XRD) analysis (Bruker Axes D2 PHASER Diffractometer) with Cu K_α radiation ($\lambda = 0.15406$ nm). The UC spectra were collected at different temperatures by using a Fluorolog-3/Jobin Yvon spectrofluorometer. A TAP-02 temperature-controlled system was used to modify the sample temperature.

XRD patterns shown in Fig. 1 are evidence that all the diffraction peaks of the samples are well indexed to the tetragonal scheelite-type phase of $BaMoO_4$. No extra impurities are detected, suggesting that Ho^{3+} and Yb^{3+} ions are incorporated into the host lattice.

Figure 2(a) shows the UC luminescence spectra of $BaMoO_4$: Ho^{3+}, Yb^{3+} samples under 980 nm excitation. The emission bands peaked at 547, 666, and 755 nm are attributed to $^5F_4/{}^5S_2 \rightarrow {}^5I_8$, $^5F_5 \rightarrow {}^5I_8$, and $^5F_4/{}^5S_2 \rightarrow {}^5I_7$ transitions, respectively. Meanwhile, the UC emission intensities are enhanced with the increasing Yb^{3+} concentration, owing to the efficient $Yb^{3+} \rightarrow Ho^{3+}$ energy transfer (ET) process, and are maximized at 7 mol% Yb^{3+} ion concentration. Beyond this, the emissions start to decline

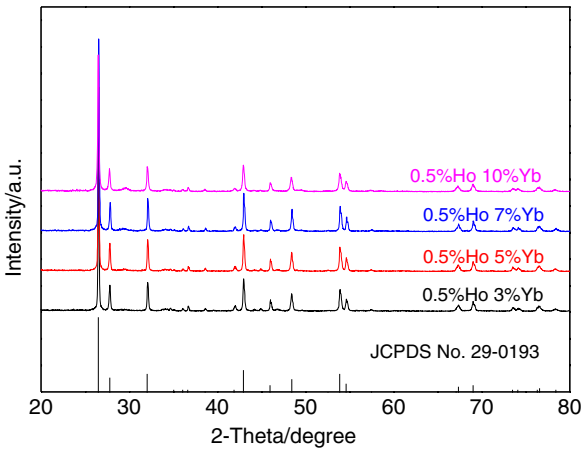

Fig. 1. XRD patterns of $BaMoO_4$: $0.5\%Ho^{3+}/x\%Yb^{3+}$ ($x = 3$, 5, 7, 10).

due to the concentration quenching effect[14]. Besides the optimal UC luminescence, an interesting IOB phenomenon is also observed for $0.5\%Ho^{3+}/7\%Yb^{3+}$: $BaMoO_4$. As shown in Fig. 2(b), the green emission intensity does not repeat a linear path with the alteration of excitation power from 300 to 1000 mW and vice versa. The presence of a hysteresis-like curve is evidence for IOB, which is associated with the cooperative ET (CET) process[8–10,15]. Due to the large concentration of Yb^{3+} ions (7 mol%) compared to that of Ho^{3+} ions (0.5 mol%) in $0.5\%Ho^{3+}/7\%Yb^{3+}$: $BaMoO_4$, large numbers of Yb^{3+} ions in the excited $^2F_{5/2}$ level can form $Yb^{3+}-Yb^{3+}$ dimmers under 980 nm excitation and transfer their energy to Ho^{3+} ions simultaneously via the CET process[15]. Consequently, an IOB behavior takes place, which may allow the phosphor to be used in optical memory devices, optical gates, and so on.

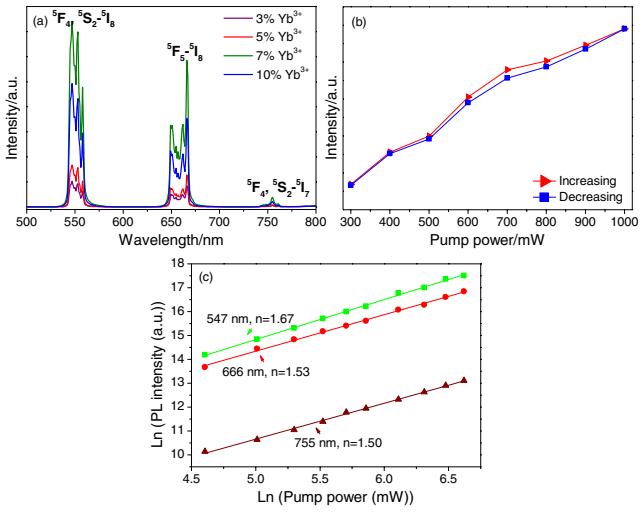

Fig. 2. (a) UC spectra of the samples under 980 nm excitation. (b) IOB plot of green emission for $BaMoO_4$: $0.5\%Ho^{3+}/7\%Yb^{3+}$ phosphor. (c) Logarithmic plots of UC emission intensities as functions of pump power.

In a UC process, the emission intensity I_{up} is proportional to the pump power (P_{NIR}) via the formula $I_{up} = P_{NIR}^n$, in which n is the number of infrared photons engaged in the UC emission[16]. From Fig. 2(c), the calculated n values indicate that two photons are involved in the green, red, and deep red UC emission processes. The deviation of the slope values from the expected photon number (−2) may result from the effect of the involved non-radiative channels (such as cross relaxation and multi-phonon relaxation) on the UC processes[17,18]. Also, as the content ratio of Yb^{3+} to Ho^{3+} is high for $0.5\%Ho^{3+}/7\%Yb^{3+}$: $BaMoO_4$, it is probable for the intermediate levels of Ho^{3+} ions to achieve saturation via absorbing energy of Yb^{3+} ions, which plays a role in the population of the upper emitting levels and leads to reduction of the slope values[19,20].

Accordingly, the UC mechanisms can be discussed with the help of an energy level diagram (Fig. 3). Since there are no energy levels of Ho^{3+} resonating with 980 nm, the UC emissions of Ho^{3+} ions mainly originate from the ET processes from Yb^{3+} to Ho^{3+} ions via two different ways. The first one is the step-by-step ET processes. Initially, Yb^{3+} ions are excited to the $^2F_{5/2}$ level via the ground state absorption (GSA) process. Then, the Ho^{3+} ions in the $^5I_8$ level are pumped to $^5F_4/^5S_2$ levels through the ET-1 and ET-2 processes. After that, the radiative transitions from the $^5F_4/^5S_2$ levels to the $^5I_8$ and $^5I_7$ ones lead to 547 and 755 nm emission, respectively. Alternatively, some Ho^{3+} ions at the $^5I_6$ level may also relax non-radiatively to the $^5I_7$ level and are further elevated to the $^5F_5$ level via the ET-3 process. Finally, the 666 nm emission occurs via the $^5F_5 \rightarrow {}^5I_8$ transition. In the second way, the CET process from the Yb^{3+} to Ho^{3+} ions contributes to the populations of the $^5F_2/^3K_8$ levels. Then, these ions non-radiatively relax to the $^5F_4/^5S_2$ levels and finally generate the 547 and 755 nm emissions.

To investigate the optical thermometric behaviors, Fig. 4(a) illustrates the temperature-dependent UC emission spectra of $BaMoO_4$: $0.5\%Ho^{3+}/7\%Yb^{3+}$ at 100 mW, which are normalized to the 666 nm peak. With temperature increment, the 547 nm emission intensity decreases

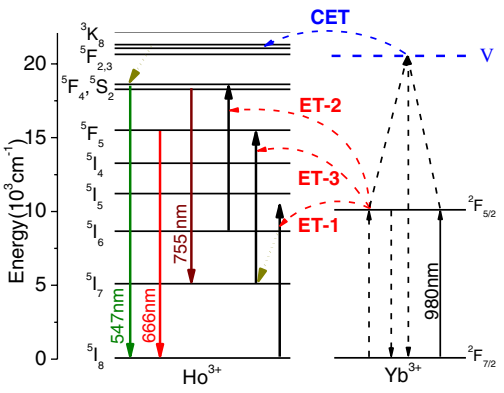

Fig. 3. Energy level diagram and the possible UC processes under 980 nm excitation.

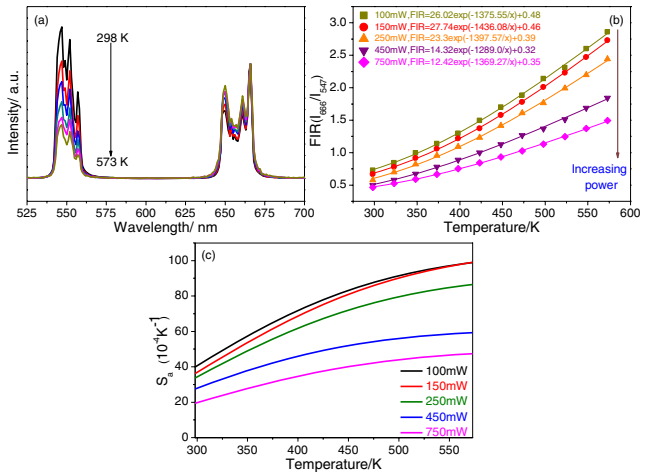

Fig. 4. (a) Temperature-dependent UC spectra. (b) The FIRs as functions of temperature under the different excitation powers. (c) The variations of S_a values with temperature and excitation power.

gradually compared to the 666 nm emission. One of the reasons is the promoted multi-phonon relaxation from the $^5F_4/^5S_2$ to the $^5F_5$ level at elevated temperatures[21,22]. Additionally, the increment of temperature also accelerates the $^5I_6 \rightarrow {}^5I_7$ non-radiative relaxation process, which is in favor of the 666 nm emission rather than the 547 nm one (Fig. 3). Hence, the 547 and 666 nm emissions are potentially for FIR thermometry due to their diverse thermal response, which has an excellent signal discriminability ($-3266\ \mathrm{cm}^{-1}$). The variations of FIRs (I_{666}/I_{547}) in the 298–573 K temperature range dependent upon different excitation powers are presented in Fig. 4(b). Clearly, the FIRs keep growing with rising temperatures, and the relation between FIR and temperature can be well fitted by the following equation:

$$\mathrm{FIR} = \frac{I_{666}}{I_{547}} = A\exp\left(\frac{-B}{T}\right) + C, \tag{1}$$

where A, B, and C are the constants related to the research system. As shown, perfect fittings can be achieved with the correlation coefficient R of up to -0.998. Therefore, the temperature can be detected based on the intensity ratio between the $^5F_5 \rightarrow {}^5I_8$ and $^5F_4/^5S_2 \rightarrow {}^5I_8$ transitions.

Then, the key parameter of absolute sensing sensitivity (S_a) can be evaluated, which is defined as $S_a = \left|\mathrm{dFIR}/\mathrm{d}T\right|$[23]. Figure 4(c) shows the maximal S_a value decreases from $99 \times 10^{-4}\ \mathrm{K}^{-1}$ to $48 \times 10^{-4}\ \mathrm{K}^{-1}$ with an increase of excitation power from 100 to 750 mW. This may be explained as follows: a high thermal sensitivity based on the $^5F_5$ and $^5F_4/^5S_2$ levels requires the efficient population of the $^5F_5$ level and depopulation of the $^5F_4/^5S_2$ levels with temperature. However, the CET process becomes more and more effective with increasing excitation power[24], which is in favor of the population of $^5F_4/^5S_2$ levels rather than the $^5F_5$ level. Consequently, FIRs (I_{666}/I_{547}) decline with the increasing excitation power [Fig. 4(b)], indicating a reducing population rate ratio between the $^5F_5$ and $^5F_4/^5S_2$ levels. Hence, the pump power increment is harmful for the thermal response of FIRs, resulting in decreasing sensitivity. The results reveal that the excitation power affects the thermometric performance remarkably, which has normally been ignored in past investigations.

In summary, a series of Ho^{3+}/Yb^{3+}: $BaMoO_4$ phosphors have been prepared and studied. Upon 980 nm excitation, $BaMoO_4$: $0.5\%Ho^{3+}/7\%Yb^{3+}$ phosphor exhibits the most intense UC emissions and an IOB behavior. Based on FIR between the $^5F_5$ and $^5F_4/^5S_2$ levels, the thermal sensitivities are found to depend on the change of excitation powers due to the impact of the CET process. Moreover, the phosphor has relatively high thermal sensitivity ($99 \times 10^{-4}\ \mathrm{K}^{-1}$) and excellent signal discriminability. The results suggest that the prepared phosphor may be applied in an optical thermometer, optical bistable device, and some other UC-based devices.

This work was supported by the Natural Science Foundation of Zhejiang Province (Nos. LY18E020008 and LD18F050001) and the National Natural Science Foundation of China (No. 61605192).

References

1. R. R. Deng, F. Qin, R. F. Chen, W. Huang, M. H. Hong, and X. G. Liu, Nat. Nanotechnol. **10**, 237 (2015).
2. M. Quintanilla and L. M. Liz-Marzán, Nano Today **19**, 126 (2018).
3. S. Ye, G. S. Wang, M. Z. Xiong, J. Song, J. L. Qu, and W. X. Xie, Chin. Opt. Lett. **15**, 011601 (2017).
4. X. J. Zhu, W. Feng, J. Chang, Y. W. Tan, J. C. Li, M. Chen, Y. Sun, and F. Y. Li, Nat. Commun. **7**, 10437 (2016).
5. A. A. Lyapin, S. V. Gushchin, A. S. Ermakov, S. V. Kuznetsov, P. A. Ryabochkina, V. Yu. Proydakova, V. V. Voronov, P. P. Fedorov, and M. V. Chernov, Chin. Opt. Lett. **16**, 091901 (2018).
6. M. Xu, D. Q. Chen, P. Huang, Z. Y. Wan, Y. Zhou, and Z. G. Ji, J. Mater. Chem. C **4**, 6516 (2016).
7. R. S. Lei, X. Y. Luo, Z. Y. Yuan, H. P. Wang, F. F. Huang, D. G. Deng, and S. Q. Xu, J. Lumin. **205**, 440 (2019).
8. M. P. Hehlen, H. U. Güdel, Q. Shu, and S. C. Rand, J. Chem. Phys. **104**, 1232 (1996).
9. A. K. Soni and V. K. Rai, Dalton Trans. **43**, 13563 (2014).
10. L. Mukhopadhyay and V. K. Rai, New J. Chem. **41**, 7650 (2017).
11. A. K. Soni, A. Kumari, and V. K. Rai, Sensor. Actuat. B Chem. **216**, 64 (2015).
12. G. Jia, C. Huang, L. Li, C. Wang, X. Song, L. Song, Z. Li, and S. Ding, Opt. Mater. **35**, 285 (2012).
13. Y. H. Xia, X. Y. Zou, H. B. Zhang, M. J. Zhao, X. Chen, W. T. Jia, C. H. Su, and J. Shao, J. Alloy. Compd. **774**, 540 (2019).
14. X. P. Li, X. Wang, H. Zhong, L. H. Cheng, S. Xu, J. S. Sun, J. S. Zhang, X. J. Li, L. L. Tong, and B. J. Chen, Ceram. Int. **42**, 14710 (2016).
15. M. Yadav, M. Mondal, L. Mukhopadhyay, and V. K. Rai, Methods Appl. Fluores. **6**, 025001 (2018).
16. X. F. Wang, Q. Liu, P. Q. Cai, J. Wang, L. Qin, T. Q. Vu, and H. J. Seo, Opt. Express **24**, 17792 (2016).
17. W. Xu, X. Y. Gao, L. J. Zheng, Z. G. Zhang, and W. W. Cao, Opt. Express **20**, 18127 (2012).

18. L. Mukhopadhyay, V. K. Rai, R. Bokolia, and K. Sreenivas, J. Lumin. **187**, 368 (2017).
19. S. Sinha, M. K. Mahata, K. Kumar, S. P. Tiwari, and V. K. Rai, Spectrochim. Acta. A **173**, 369 (2017).
20. S. F. Liu, H. Ming, J. Cui, S. B. Liu, W. X. You, X. Y. Ye, Y. M. Yang, H. P. Nie, and R. X. Wang, J. Phys. Chem. C **122**, 16289 (2018).
21. J. Zhang, Y. Q. Zhang, and X. M. Jiang, J. Alloy. Compd. **748**, 438 (2018).
22. J. Zhang, X. M. Jiang, and Z. H. Hua, Ind. Eng. Chem. Res. **57**, 7507 (2018).
23. M. D. Dramićanin, Methods Appl. Fluores. **4**, 042001 (2016).
24. R. S. Yadav, S. J. Dhobleb, and S. B. Rai, Methods Appl. Fluores. **42**, 7272 (2018).